ARTICLES

Brain metabolism dictates the polarity of astrocyte control over arterioles

Grant R. J. Gordon[1], Hyun B. Choi[1], Ravi L. Rungta[1], Graham C. R. Ellis-Davies[2] & Brian A. MacVicar[1]

Calcium signalling in astrocytes couples changes in neural activity to alterations in cerebral blood flow by eliciting vasoconstriction or vasodilation of arterioles. However, the mechanism for how these opposite astrocyte influences provide appropriate changes in vessel tone within an environment that has dynamic metabolic requirements remains unclear. Here we show that the ability of astrocytes to induce vasodilations over vasoconstrictions relies on the metabolic state of the rat brain tissue. When oxygen availability is lowered and astrocyte calcium concentration is elevated, astrocyte glycolysis and lactate release are maximized. External lactate attenuates transporter-mediated uptake from the extracellular space of prostaglandin E_2, leading to accumulation and subsequent vasodilation. In conditions of low oxygen concentration extracellular adenosine also increases, which blocks astrocyte-mediated constriction, facilitating dilation. These data reveal the role of metabolic substrates in regulating brain blood flow and provide a mechanism for differential astrocyte control over cerebrovascular diameter during different states of brain activation.

In the brain, regional changes in neural activity trigger localized alterations in cerebral blood flow[1] through astrocyte activation[2,3]. A rise in intracellular free calcium concentration ($[Ca^{2+}]_i$) within astrocyte endfeet, which collectively circumscribe all cerebral vessels[4], initiates vasoconstriction[5–7] or vasodilation[2,6,8–10]. Cerebral blood flow couples to the lactate/pyruvate ratio and the related nicotinamide adenine dinucleotide (NADH)/NAD^+ ratio[11–13], but links between these metabolic substrates and the mechanisms of cerebral blood flow regulation remain unresolved. We tested the hypothesis that the metabolic state of the tissue, altered by oxygen (O_2) availability, dictates the type of astrocyte influence on arteriole diameter. At the onset of neural activity dendrites rapidly consume O_2 (ref. 14), leading to a reduction in oxygen pressure (p_{O2})[15–17] and oxyhaemoglobin[18,19], which occurs before the increase in cerebral blood flow. Brain metabolism then shifts, whereby glycolysis is enhanced[20,21] in astrocytes[14] and lactate is released[22,23]. Lactate is vasoactive[12,24] and dynamically alters microvasculature diameter in an O_2-dependent manner[25]. Vasodilation occurs in the brain region experiencing the O_2 drop, whereas vasoconstriction ensues in the inactive surrounding area[26]. Delineating the cellular processes responsible for O_2-metabolic effects on cerebral blood flow may be crucial for treating stroke and vascular dementia, as well as aiding in our understanding of neurovascular coupling for the scientific and diagnostic uses of functional magnetic resonance imaging.

p_{O2} converts polarity of vessel response

We tested whether p_{O2} consistently determined if vasoconstrictions or vasodilations were evoked by synaptic activation or by astrocyte Ca^{2+} transients in rat brain slices. In response to periodic 10–20-Hz stimulation of the hippocampal CA3–CA1 pathway in conditions of high O_2 concentration (95%) arterioles constricted ($81.4 \pm 3.8\%$ (100% = control diameter), $n = 6$, $P < 0.007$), whereas the same vessel in low O_2 concentration (20%) dilated ($107.6 \pm 0.7\%$, $n = 6$, $P < 0.005$, $P < 0.0003$ to each other, Fig. 1a–c) in response to the same stimulation. To determine the impact of p_{O2} on astrocyte control of arteriole diameter we applied the metabotropic glutamate receptor (mGluR) agonist (±)-1-aminocyclopentane-trans-1,3-dicarboxylic acid (tACPD) (100 μM), which potently increased astrocyte $[Ca^{2+}]_i$[2,5,8] ($240.0 \pm 19.1\%$, $n = 14$, $P < 0.001$, Fig. 2a) and caused arteriole dilation in conditions of low O_2 concentration ($107.0 \pm 0.8\%$, $n = 23$, $P < 0.001$, Fig. 2a, f) but constriction in conditions of high O_2 concentration[5] ($85.4 \pm 4.0\%$, $n = 10$, $P < 0.006$, Fig. 2f). Next we used two-photon photolysis of the Ca^{2+} cage dimethoxy-nitrophenyl-EGTA-4 (DMNPE-4)[27] to liberate directly astrocyte Ca^{2+} and examine the vessel response. Uncaging DMNPE-4 triggered a Ca^{2+} wave that spread to multiple astrocyte endfeet (Fig. 2b, c). In contrast to previous results in conditions of high O_2 concentration where astrocyte endfeet Ca^{2+} caused constriction[5], in conditions of low O_2 endfeet Ca^{2+} ($232.2 \pm 8.5\%$, $n = 17$, $P < 0.001$) caused dilation ($107.4 \pm 1.0\%$, $n = 17$, $P < 0.003$, Fig. 2b, c, f). These data indicate that p_{O2} dictates the direction of arteriole diameter change when astrocytes are activated (Supplementary Fig. 2 for p_{O2} measurements).

Vasodilation requires COX and PGE_2

Astrocyte Ca^{2+} activates cytosolic phospholipase A_2, triggering formation of arachidonic acid that is either converted to 20-hydroxyeicosatetraenoic acid (20-HETE) in smooth muscle cells causing vasoconstriction[5] or to the vasodilator prostaglandin E_2 (PGE_2) in astrocytes via cyclooxygenase (COX)[2,9]. We verified COX1 and COX2 expression in astrocytes and their endfeet (Supplementary Fig. 3). The COX inhibitor indomethacin (100 μM) blocked vasodilations caused by tACPD ($98.4 \pm 0.8\%$, $n = 9$, $P < 0.0001$ to tACPD alone, Fig. 2f) and by caged Ca^{2+} photolysis ($101.0 \pm 0.5\%$, $n = 6$, $P < 0.002$ to uncaging alone, Fig. 2d, f) in conditions of low O_2 concentration. Application of the COX product PGE_2 (1 μM) elicited vasodilation ($109.4 \pm 2.7\%$, $n = 4$, $P < 0.05$, Fig. 2e), confirming COX activation and that the generation of PGE_2 is an important signalling molecule in astrocyte-mediated vasodilations in conditions of low O_2 concentration[2,9].

We investigated how changing p_{O2} could modify the type of astrocyte influence on arterioles. Lowering p_{O2} may elevate anaerobic

[1]Brain Research Centre, Department of Psychiatry, University of British Columbia, British Columbia T2N 2B5, Canada. [2]Department of Pharmacology & Physiology, Drexel University College of Medicine, Philadelphia, Pennsylvania 19102, USA.

©2008 Macmillan Publishers Limited. All rights reserved

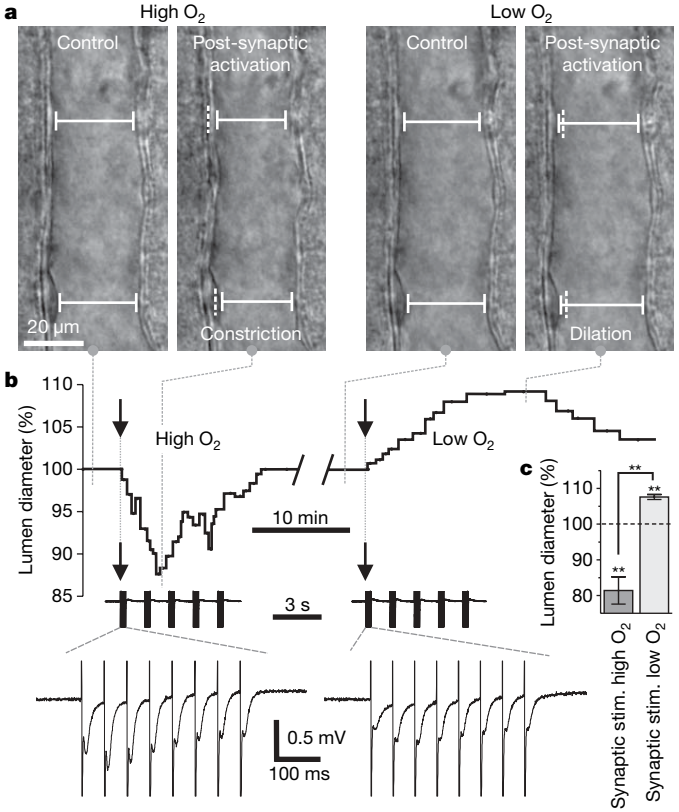

Figure 1 | Lowering p_{O2} converts vasoconstriction to vasodilation. **a**, Arteriole before and after synaptic activation in high O_2 (left) and low O_2 (right). Dashed vertical lines indicate the previous position of the vessel wall. **b**, Top: vessel lumen diameter changes over time in the same vessel shown in **a**. Arrows indicate time of afferent stimulation. Bottom: two expanded timescales show the stimulation protocol (350-ms, 20-Hz train repeated 5 times at 0.75 Hz) and the first train of the field excitatory postsynaptic potentials evoked, verifying synaptic activity. **c**, Summary data ($n = 6$). In all figures, experimental values are the mean ± s.e.m. Double asterisk, $P < 0.01$.

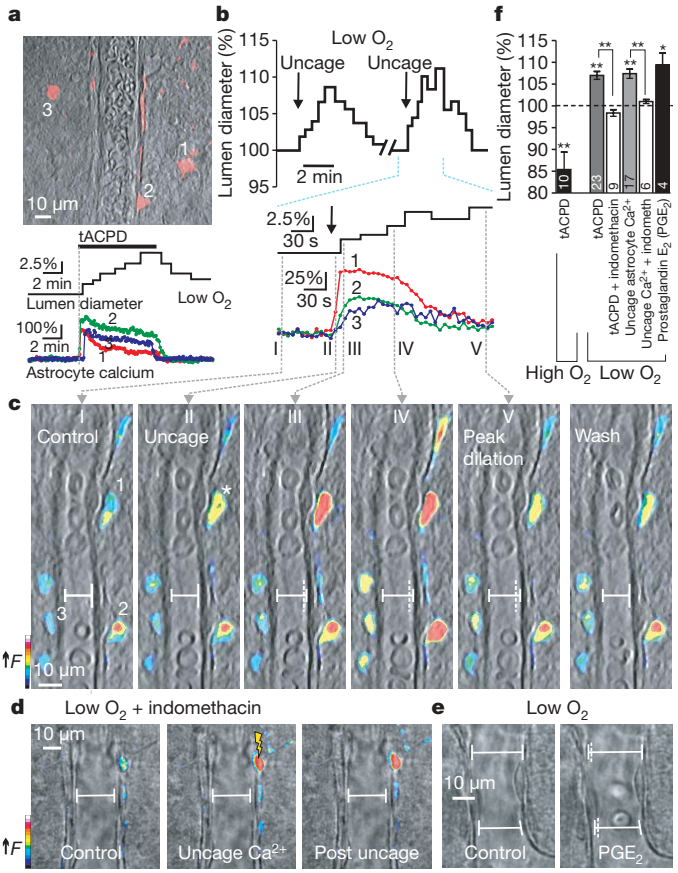

Figure 2 | O_2-mediated conversion to astrocyte-mediated vasodilation requires COX and PGE_2. **a**, Top: astrocytes (red) surround arteriole. Bottom: astrocyte Ca^{2+} signals occur coincident with vasodilation caused by the mGluR agonist tACPD in low O_2. **b**, Top: uncaging astrocyte Ca^{2+} causes vasodilation in low O_2. Bottom: expanded timescale shows that astrocyte endfoot Ca^{2+} precedes diameter increase. **c**, Vessel and pseudo-coloured endfoot Ca^{2+} changes corresponding to times in **b**. **d**, Blocking COX prevents vasodilation caused by uncaging Ca^{2+} in low O_2. **e**, PGE_2 causes vasodilation in low O_2. **f**, Summary data. Asterisk, $P < 0.05$; double asterisk, $P < 0.01$.

metabolism, increasing external lactate. Notably, the action of PGE_2 is terminated when prostaglandin transporters (PGTs) take up PGE_2 by an exchange of intracellular lactate[28]. Owing to the influence of a lactate concentration gradient on PGT efficacy, we tested the hypothesis that higher levels of extracellular lactate reduce PGT uptake of PGE_2, thereby increasing the external PGE_2 concentration resulting in vasodilation. Immunohistochemistry revealed that PGT was expressed in astrocyte endfeet (Fig. 3a) and neurons (Fig. 3b), indicating that both cell types take up PGE_2. Consistent with a positive correlation between external lactate and external PGE_2, low O_2 concentration enhanced both lactate release (low O_2, 114.2 ± 9.1 μM, $n = 6$; high O_2, 41.9 ± 5.6 μM, $n = 6$, $P < 0.001$, Fig. 3c) and extracellular PGE_2 levels when PGE_2 production was triggered by tACPD (low O_2, 136.1 ± 10.2 pg ml^{-1}, $n = 6$; high O_2, 91.9 ± 12.6 pg ml^{-1}, $n = 4$, $P < 0.001$, Fig. 3d). Addition of lactate (1 mM) enhanced the PGE_2 level (control, 40.5 ± 3.3 pg ml^{-1}; with lactate, 58.0 ± 3.1 pg ml^{-1}, $n = 5$, $P < 0.01$) and increased arteriole diameter (107.5 ± 1.0%, $n = 15$, $P < 0.0001$, Fig. 3e–g). Lactate-induced dilations were blocked by indomethacin (100.4 ± 0.4%, $n = 11$, $P < 0.0001$ to lactate alone, Fig. 3g), indicating that they were mediated by PGE_2 via the COX pathway. These data indicate that in low O_2 concentration higher levels of extracellular lactate raise external levels of PGE_2.

Vasodilation requires lactate

We examined the role of astrocyte glycolysis in lactate production[23,29] by imaging the intrinsic fluorescence of the metabolic electron carrier NADH[30]. Two-photon excitation of NADH provides a measure of both oxidative metabolism (punctate mitochondrial fluorescence) and glycolytic metabolism (diffuse cytosolic fluorescence)[14]. We observed that astrocytes, stained with SR-101 (ref. 31), showed diffuse NADH fluorescence in the soma and endfeet (Fig. 3h, i). Stimulating glycolysis with low O_2 increased the astrocyte NADH signal (124.6 ± 1.4%, $n = 5$, $P < 0.003$, Fig. 3i, j) and inhibiting glycolysis with iodoacetate (200 μM) reduced basal NADH levels (87.8 ± 2.0%, $n = 5$, $P < 0.004$, Fig. 3k). Inhibiting lactate dehydrogenase (LDH, which converts pyruvate and NADH to lactate and NAD^+; Supplementary Fig. 1) with oxamate (2.5 mM) increased NADH (119.3 ± 2.0%, $n = 6$, $P < 0.004$, Fig. 3l). These data indicate that astrocyte glycolysis can be augmented by reducing p_{O2}.

Recent two-photon NADH imaging demonstrated an increase in astrocyte glycolysis caused by neuronal activity[14]. We proposed that mGluR activation enhances astrocyte glycolysis in conditions of low O_2, promoting increases in extracellular lactate and vasodilation. tACPD triggered an increase in astrocyte NADH (128.7 ± 4.1%, $n = 7$, $P < 0.0005$, Fig. 4a–e) coincident with lumen widening (108.5 ± 0.7%, $n = 7$, $P < 0.01$, Fig. 4b, c). tACPD enhanced extracellular lactate, which was greatest in low O_2 (low O_2, 186.7 ± 11.2 μM, $n = 6$; high O_2, 98.6 ± 10.2 μM, $n = 7$, $P < 0.001$, Fig. 4f). For additional NADH measurements see Supplementary Figs 4 and 5. We used two pharmacological treatments to limit lactate

©2008 Macmillan Publishers Limited. All rights reserved

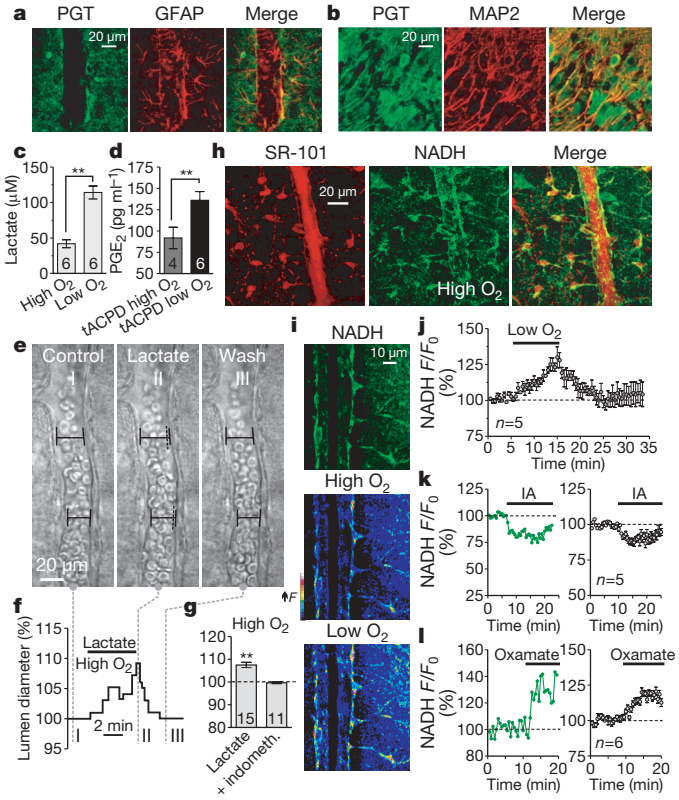

Figure 3 | Low O_2 facilitates lactate and PGE_2 release and enhances astrocyte glycolysis. **a**, **b**, Immunohistochemistry showing that astrocyte endfeet and neurons express PGT. **c**, Lactate release is elevated in conditions of low O_2. **d**, tACPD increases PGE_2 release most in conditions of low O_2. **e**–**g**, Lactate dilates arterioles and requires COX. Double asterisk, $P < 0.01$. **h**, Metabolic NADH signal (green image stack) in astrocytes (red image stack). **i**, Low O_2 increases NADH signal. **j**, Astrocyte NADH changes caused by low O_2. **k**, **l**, Astrocyte NADH in response to glycolysis inhibition with iodoacetate (IA, **k**) or LDH inhibition with oxamate (**l**). Green traces are single experiments; grey traces are summary data.

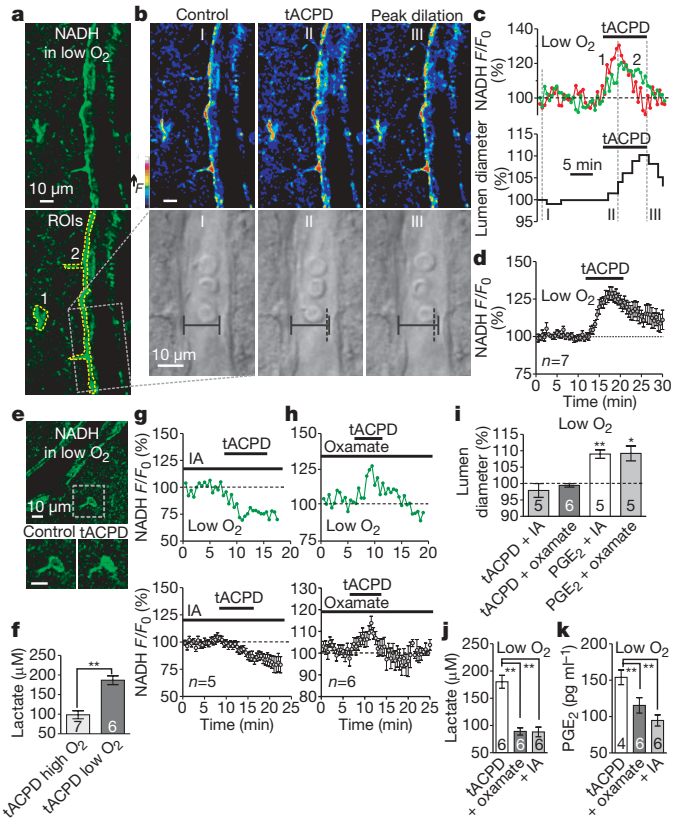

Figure 4 | Glycolysis and lactate release is required for vasodilations. **a**–**d**, Astrocyte NADH increases (measurements from the regions of interest (ROIs)) coincident with vasodilation in response to tACPD in low O_2. **e**, tACPD increases cytosolic NADH in astrocytes. **f**, tACPD increases extracellular lactate most in conditions of low O_2. **g**, tACPD decreases astrocyte NADH during glycolysis inhibition with iodoacetate (IA). **h**, tACPD increases astrocyte NADH during LDH inhibition with oxamate. Green traces are single experiments; grey traces are summary data. **i**, tACPD fails to dilate vessels in the presence of oxamate or iodoacetate, and PGE_2 rescues vasodilation in these compounds. **j**, **k**, The increase in lactate and PGE_2 levels caused by tACPD is reduced in oxamate and iodoacetate.

release. Using iodoacetate to block the source of lactate, tACPD instead decreased astrocyte NADH (81 ± 0.4%, $n = 5$, $P < 0.0001$ to tACPD alone, Fig. 4g) and failed to dilate vessels (97.8 ± 0.2%, $n = 5$, $P < 0.0001$ to tACPD alone, Fig. 4i). The NADH signal decrease was probably due to tACPD-induced astrocyte swelling. Using oxamate to curtail lactate formation, tACPD still increased astrocyte NADH (112.8 ± 3.1%, $n = 6$, $P < 0.02$, Fig. 4h; see Supplementary Fig. 1), yet vasodilations no longer occurred (99.0 ± 0.1%, $n = 6$, $P < 0.0001$ to tACPD alone, Fig. 4i). The lack of dilation was associated with reduced extracellular lactate (tACPD, 180.2 ± 11.9 μM, $n = 6$; plus iodoacetate, 88.2 ± 8.8 μM, $n = 6$, $P < 0.001$; plus oxamate, 89.1 ± 6.6 μM, $n = 6$, $P < 0.001$, Fig. 4j) and PGE_2 (tACPD, 154.0 ± 10.1 pg ml^{-1}, $n = 4$; plus iodoacetate, 115.4 ± 10.6 pg ml^{-1}, $n = 6$, $P < 0.001$; plus oxamate, 94.6 ± 7.6 pg ml^{-1}, $n = 6$, $P < 0.01$, Fig. 4k). Because PGE_2 is the final effector molecule on smooth muscle cells, we rescued vasodilation with PGE_2 in iodoacetate (109.0 ± 1.3%, $P < 0.002$, $n = 5$, Fig. 4i) or in oxamate (109.2 ± 2.2%, $P < 0.02$, $n = 5$, Fig. 4i and Supplementary Fig. 6). These data demonstrate that inhibition of glycolysis or LDH limits extracellular lactate and PGE_2 accumulation in response to tACPD in low O_2 conditions, preventing astrocyte-mediated vasodilations.

Adenosine blocks vasoconstriction

Our data do not yet explain why vasoconstrictions are absent in low O_2. A low-O_2 environment causes an elevation in extracellular adenosine[32,33], and adenosine A2A receptors reduce smooth muscle cell Ca^{2+} channel activity[34], which normally acts to induce smooth muscle cell contraction. We hypothesized that A2A receptor activation prevents astrocyte-mediated vasoconstriction. Adenosine also suppresses synaptic glutamate release through the A1 receptor[33]; thus, we confirmed an elevated adenosine concentration in low O_2 when the A1 receptor antagonist 8-cyclopentyl-1,3-dipropylxanthine (DPCPX; 100 nM) increased the slope of the extracellular field potential (low O_2, 277.7 ± 63.6%, $n = 9$; high O_2, 99.1 ± 7.1%, $P < 0.05$, $n = 5$, Fig. 5a) and decreased the paired-pulse ratio (low O_2, 1.79 ± 0.04; plus DPCPX, 1.42 ± 0.05, $P < 0.0001$, $n = 9$; high O_2, 1.47 ± 0.01; plus DPCPX, 1.49 ± 0.03, $P > 0.5$, $n = 5$, Fig. 5a) only in low O_2. In the presence of adenosine (100 μM), uncaging astrocyte Ca^{2+} in high O_2 concentration resulted in no vasoconstriction (99.6 ± 0.9%, $P > 0.6$, $n = 4$, Supplementary Fig. 7). After an initial uncaging event that caused constriction (87.1 ± 1.3%, $P < 0.002$, Fig. 5b), the A2A receptor agonist CGS21680 (1 μM) blocked subsequent constriction (99.3 ± 0.5%, $P < 0.0004$ to constriction, $n = 7$, Fig. 5b) despite similar astrocyte Ca^{2+} signals ($F/F_0 = 179.9 \pm 10.9\%$; plus CGS21680 $F/F_0 = 173.8 \pm 10.3\%$, $n = 7$, $P > 0.7$). A2A receptor activation did not affect PGE_2 in response to tACPD (217.0 ± 20.4%, $n = 5$; plus CGS21680, 186.6 ± 12.1%, $n = 6$, $P > 0.2$), allowing vasodilations to proceed in low O_2. These data demonstrate that increasing extracellular adenosine levels, which occurs in low O_2, prevents astrocyte-mediated vasoconstriction, thereby facilitating the switch to vasodilation.

©2008 Macmillan Publishers Limited. All rights reserved

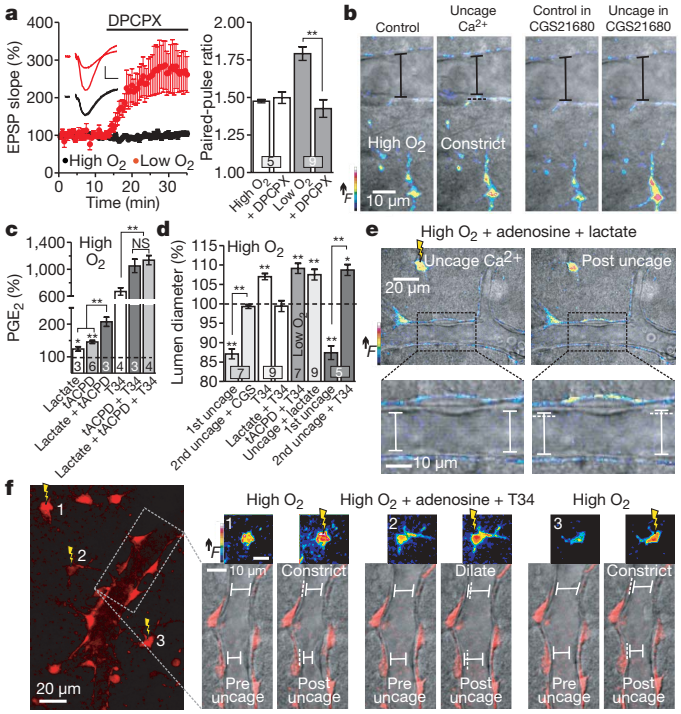

Figure 5 | Raising adenosine and PGE_2 levels converts the vessel response. **a**, Enhancement of synaptic transmission by DPCPX shows that extracellular adenosine is elevated in conditions of low O_2 concentration. Scale bars: 0.3 mV, 5 ms. EPSP, excitatory postsynaptic potential. **b**, In conditions of high O_2 concentration uncaging Ca^{2+} fails to cause vasoconstriction in the presence of the A2A receptor agonist CGS21680. **c**, T34 blocks lactate from increasing PGE_2 levels. NS, not significant. **d**, Summary of vessel responses. Values for lactate plus T34 and tACPD plus T34 were normalized to T34 baseline. **e**, In conditions of high O_2 concentration uncaging Ca^{2+} in adenosine and lactate triggers vasodilation instead of vasoconstriction. **f**, In conditions of high O_2 concentration vessel responses caused by uncaging Ca^{2+} convert from vasoconstriction to vasodilation in the presence of adenosine and T34.

Lactate attenuates PGT efficacy

We pharmacologically inhibited PGTs to raise extracellular levels of PGE_2 and examine the effect on arterioles. Blockade of PGTs with TGBz T34 (ref. 35) (hereafter called T34) (20 μM) elevated PGE_2 levels (669.0 ± 110.8%, $P < 0.0001$, $n = 4$, Fig. 5c) and dilated arterioles (107.0 ± 0.8%, $P < 0.001$, $n = 7$, Fig. 5d), indicating tonic PGE_2 uptake. Adding tACPD further enhanced the PGE_2 level (T34 plus tACPD, 1,048.9 ± 173.6%, $P < 0.02$ compared to T34, $n = 3$, Fig. 5c) and caused further dilation (T34 plus tACPD, 109.1 ± 1.3%, $P < 0.0004$ from T34 baseline, $n = 7$, Fig. 5d), indicating that PGE_2 release occurs by diffusion and not by the transporter[36]. However, adding lactate did not further augment PGE_2 (T34 plus tACPD plus lactate, 1,134.2 ± 138.7%, $P > 0.4$ compared to T34 plus tACPD, $n = 4$, Fig. 5c) in contrast to the additive effects of lactate and tACPD without T34 (lactate, 124.0 ± 11.9%, $P < 0.02$, $n = 3$; tACPD, 145.6 ± 11.6%, $P < 0.001$, $n = 6$; lactate plus tACPD, 207.0 ± 24.3%, $n = 3$, $P < 0.005$ to tACPD or lactate alone, Fig. 5c). Dilation caused by T34 was not increased further by lactate (T34 plus lactate, 99.4 ± 1.4%, $P > 0.1$ from T34 baseline, $n = 9$, Fig. 5d). These data indicate that T34 occludes the lactate effects of raising PGE_2 and causing vasodilation. This demonstrates that PGT efficacy controls the PGE_2 level and thus vascular tone.

PGE_2 and adenosine convert constrictions

We reasoned that adding lactate (100 μM to 1 mM) and adenosine (100 μM) in conditions of high O_2 would enable astrocyte-mediated constrictions to convert to dilations by attenuating PGE_2 uptake and blocking vasoconstriction, respectively. Under this condition, Ca^{2+} uncaging now resulted in dilation (107.5 ± 1.4%, $P < 0.004$ to adenosine alone, $n = 9$, Fig. 5d, e), despite equivalent Ca^{2+} signals in astrocyte endfeet compared with adenosine alone (adenosine, $F/F_0 = 160.4 \pm 6.1\%$, $n = 4$; plus lactate, $F/F_0 = 159.6 \pm 5.1\%$, $P > 0.8$, $n = 9$, Supplementary Fig. 7). We hypothesized that PGT blockade by T34 in high O_2 would have a similar result by reducing PGE_2 uptake, thereby raising extracellular PGE_2. In the same vessel, an initial uncaging event caused constriction (87.4 ± 1.8%, $P < 0.009$, Fig. 5d, f) but a second uncaging event in the presence of T34 and adenosine caused dilation (108.7 ± 1.4%, $n = 5$, $P < 0.02$, $P < 0.0001$ to constriction, Fig. 5d, f). These data indicate that astrocytes induce vasodilation over vasoconstriction when constrictions are prevented by adenosine and PGE_2 uptake is reduced by elevated lactate.

Here we show that by lowering p_{O2}, astrocyte-induced responses convert to vasodilations from vasoconstrictions. Astrocyte Ca^{2+} transients from mGluR activation trigger the synthesis of diffusible arachidonic acid and PGE_2. In high O_2, extracellular PGE_2 is rapidly cleared by PGTs as a result of low extracellular lactate levels. This keeps extracellular PGE_2 levels low and allows astrocyte-derived arachidonic acid to constrict arterioles[5]. In low O_2, astrocyte glycolysis is enhanced and extracellular lactate increases. High external lactate hinders PGE_2 clearance and increases extracellular PGE_2, which dilates arterioles. In addition, increased adenosine release in low O_2 inhibits astrocyte-mediated vasoconstrictions at the level of smooth muscle cells, blocking the effect of arachidonic acid (Supplementary Fig. 1). Flow through blood vessels is proportional to vessel radius to the fourth power; therefore, a ~9% change in arteriole diameter reported here equates to a ~45% increase in cerebral blood flow. This change is consistent with astrocyte-mediated vasodilations observed *in vivo*[8] and can account for cerebral blood flow changes measured by positron emission tomography[37] and with two-photon microscopy[38,39] during physiological activation. Previous studies on the bidirectional control of vessel diameter implicated different populations of GABA neurons[40], nitric oxide levels[6] and pericytes[41]. Our data indicate that the separate yet competing molecular pathways regulating cerebral blood flow from astrocytes would reach an equilibrium, which shifts depending on the degree of metabolic activity. Under more quiescent periods when O_2 is not being rapidly consumed, astrocyte Ca^{2+} signals induce constrictor tone, keeping cerebral blood flow at an appropriate lower level. During more active periods, the drop in p_{O2} from oxygen consumption and the rise in extracellular lactate and adenosine promote astrocyte-mediated dilation. Manipulating this balance may be a therapeutic avenue for treating the inappropriate declines in cerebral blood flow that occur in some dementias and after stroke.

METHODS SUMMARY

Hippocampal–neocortical slices were prepared from juvenile (postnatal age 16–21 days), male, Sprague–Dawley rats. Treatment of animals was approved by the University of British Columbia Animal Care and Use Committee. Artificial cerebrospinal fluid (ACSF) bubbled with 95% O_2, 5% CO_2, was defined as high O_2 and 20% O_2, 5% CO_2, balanced N_2, was defined as low O_2. Astrocytes were loaded with the Ca^{2+} cage DMNPE-4/AM (10 μM) and/or the Ca^{2+} indicator rhod-2/AM (10 μM) as previously described[5]. A two-photon laser-scanning microscope (Zeiss LSM510-Axioskop-2 fitted with a 40X-W/0.80 numerical aperture objective lens) coupled to a Chameleon ultra-tunable ultra-fast laser (~100-fs pulses 76 MHz, Coherent) provided excitation of rhod-2, intrinsic NADH and was used for uncaging Ca^{2+}. Arterioles were imaged by acquiring the transmitted laser light and using IR-DIC optics. Quantification of lumen diameter, NADH and Ca^{2+} changes were performed with Zeiss LSM (version 3.2) software and ImageJ. The assay used for measuring PGE_2 release was Specific Parameter PGE_2 ELISA kits (R&D systems). Extracellular lactate levels were measured using a lactate assay kit (Biomedical Research Service Centre). Experimental values are the mean ± s.e.m., expressed as a percentage of 100% control.

©2008 Macmillan Publishers Limited. All rights reserved

Full Methods and any associated references are available in the online version of the paper at www.nature.com/nature.

Received 1 April; accepted 10 October 2008.
Published online 29 October 2008.

1. Mukamel, R. *et al.* Coupling between neuronal firing, field potentials, and FMRI in human auditory cortex. *Science* **309,** 951–954 (2005).
2. Zonta, M. *et al.* Neuron-to-astrocyte signaling is central to the dynamic control of brain microcirculation. *Nature Neurosci.* **6,** 43–50 (2003).
3. Schummers, J., Yu, H. & Sur, M. Tuned responses of astrocytes and their influence on hemodynamic signals in the visual cortex. *Science* **320,** 1638–1643 (2008).
4. Simard, M., Arcuino, G., Takano, T., Liu, Q. S. & Nedergaard, M. Signaling at the gliovascular interface. *J. Neurosci.* **23,** 9254–9262 (2003).
5. Mulligan, S. J. & MacVicar, B. A. Calcium transients in astrocyte endfeet cause cerebrovascular constrictions. *Nature* **431,** 195–199 (2004).
6. Metea, M. R. & Newman, E. A. Glial cells dilate and constrict blood vessels: a mechanism of neurovascular coupling. *J. Neurosci.* **26,** 2862–2870 (2006).
7. Chuquet, J., Hollender, L. & Nimchinsky, E. A. High-resolution *in vivo* imaging of the neurovascular unit during spreading depression. *J. Neurosci.* **27,** 4036–4044 (2007).
8. Filosa, J. A., Bonev, A. D. & Nelson, M. T. Calcium dynamics in cortical astrocytes and arterioles during neurovascular coupling. *Circ. Res.* **95,** e73–e81 (2004).
9. Takano, T. *et al.* Astrocyte-mediated control of cerebral blood flow. *Nature Neurosci.* **9,** 260–267 (2006).
10. Filosa, J. A. *et al.* Local potassium signaling couples neuronal activity to vasodilation in the brain. *Nature Neurosci.* **9,** 1397–1403 (2006).
11. Mintun, M. A., Vlassenko, A. G., Rundle, M. M. & Raichle, M. E. Increased lactate/pyruvate ratio augments blood flow in physiologically activated human brain. *Proc. Natl Acad. Sci. USA* **101,** 659–664 (2004).
12. Ido, Y., Chang, K. & Williamson, J. R. NADH augments blood flow in physiologically activated retina and visual cortex. *Proc. Natl Acad. Sci. USA* **101,** 653–658 (2004).
13. Vlassenko, A. G., Rundle, M. M., Raichle, M. E. & Mintun, M. A. Regulation of blood flow in activated human brain by cytosolic NADH/NAD^+ ratio. *Proc. Natl Acad. Sci. USA* **103,** 1964–1969 (2006).
14. Kasischke, K. A., Vishwasrao, H. D., Fisher, P. J., Zipfel, W. R. & Webb, W. W. Neural activity triggers neuronal oxidative metabolism followed by astrocytic glycolysis. *Science* **305,** 99–103 (2004).
15. Vanzetta, I. & Grinvald, A. Increased cortical oxidative metabolism due to sensory stimulation: implications for functional brain imaging. *Science* **286,** 1555–1558 (1999).
16. Ances, B. M., Buerk, D. G., Greenberg, J. H. & Detre, J. A. Temporal dynamics of the partial pressure of brain tissue oxygen during functional forepaw stimulation in rats. *Neurosci. Lett.* **306,** 106–110 (2001).
17. Offenhauser, N., Thomsen, K., Caesar, K. & Lauritzen, M. Activity-induced tissue oxygenation changes in rat cerebellar cortex: interplay of postsynaptic activation and blood flow. *J. Physiol.* **565,** 279–294 (2005).
18. Malonek, D. *et al.* Vascular imprints of neuronal activity: relationships between the dynamics of cortical blood flow, oxygenation, and volume changes following sensory stimulation. *Proc. Natl Acad. Sci. USA* **94,** 14826–14831 (1997).
19. Devor, A. *et al.* Coupling of the cortical hemodynamic response to cortical and thalamic neuronal activity. *Proc. Natl Acad. Sci. USA* **102,** 3822–3827 (2005).
20. Fox, P. T. & Raichle, M. E. Focal physiological uncoupling of cerebral blood flow and oxidative metabolism during somatosensory stimulation in human subjects. *Proc. Natl Acad. Sci. USA* **83,** 1140–1144 (1986).
21. Fox, P. T., Raichle, M. E., Mintun, M. A. & Dence, C. Nonoxidative glucose consumption during focal physiologic neural activity. *Science* **241,** 462–464 (1988).
22. Hu, Y. & Wilson, G. S. A temporary local energy pool coupled to neuronal activity: fluctuations of extracellular lactate levels in rat brain monitored with rapid-response enzyme-based sensor. *J. Neurochem.* **69,** 1484–1490 (1997).
23. Pellerin, L. & Magistretti, P. J. Glutamate uptake into astrocytes stimulates aerobic glycolysis: a mechanism coupling neuronal activity to glucose utilization. *Proc. Natl Acad. Sci. USA* **91,** 10625–10629 (1994).
24. Hein, T. W., Xu, W. & Kuo, L. Dilation of retinal arterioles in response to lactate: role of nitric oxide, guanylyl cyclase, and ATP-sensitive potassium channels. *Invest. Ophthalmol. Vis. Sci.* **47,** 693–699 (2006).
25. Yamanishi, S., Katsumura, K., Kobayashi, T. & Puro, D. G. Extracellular lactate as a dynamic vasoactive signal in the rat retinal microvasculature. *Am. J. Physiol. Heart Circ. Physiol.* **290,** H925–H934 (2006).
26. Devor, A. *et al.* Suppressed neuronal activity and concurrent arteriolar vasoconstriction may explain negative blood oxygenation level-dependent signal. *J. Neurosci.* **27,** 4452–4459 (2007).
27. Ellis-Davies, G. C. Caged compounds: photorelease technology for control of cellular chemistry and physiology. *Nature Methods* **4,** 619–628 (2007).
28. Chan, B. S., Endo, S., Kanai, N. & Schuster, V. L. Identification of lactate as a driving force for prostanoid transport by prostaglandin transporter PGT. *Am. J. Physiol. Renal Physiol.* **282,** F1097–F1102 (2002).
29. Wender, R. *et al.* Astrocytic glycogen influences axon function and survival during glucose deprivation in central white matter. *J. Neurosci.* **20,** 6804–6810 (2000).
30. Chance, B., Cohen, P., Jobsis, F. & Schoener, B. Intracellular oxidation-reduction states *in vivo*. *Science* **137,** 499–508 (1962).
31. Nimmerjahn, A., Kirchhoff, F., Kerr, J. N. & Helmchen, F. Sulforhodamine 101 as a specific marker of astroglia in the neocortex *in vivo*. *Nature Methods* **1,** 31–37 (2004).
32. Frenguelli, B. G., Llaudet, E. & Dale, N. High-resolution real-time recording with microelectrode biosensors reveals novel aspects of adenosine release during hypoxia in rat hippocampal slices. *J. Neurochem.* **86,** 1506–1515 (2003).
33. Brust, T. B., Cayabyab, F. S., Zhou, N. & MacVicar, B. A. p38 mitogen-activated protein kinase contributes to adenosine A1 receptor-mediated synaptic depression in area CA1 of the rat hippocampus. *J. Neurosci.* **26,** 12427–12438 (2006).
34. Murphy, K. *et al.* Adenosine-A2a receptor down-regulates cerebral smooth muscle L-type Ca^{2+} channel activity via protein tyrosine phosphatase, not cAMP-dependent protein kinase. *Mol. Pharmacol.* **64,** 640–649 (2003).
35. Chi, Y., Khersonsky, S. M., Chang, Y. T. & Schuster, V. L. Identification of a new class of prostaglandin transporter inhibitors and characterization of their biological effects on prostaglandin E2 transport. *J. Pharmacol. Exp. Ther.* **316,** 1346–1350 (2006).
36. Chan, B. S., Satriano, J. A., Pucci, M. & Schuster, V. L. Mechanism of prostaglandin E2 transport across the plasma membrane of HeLa cells and *Xenopus* oocytes expressing the prostaglandin transporter 'PGT'. *J. Biol. Chem.* **273,** 6689–6697 (1998).
37. Fox, P. T. & Raichle, M. E. Stimulus rate dependence of regional cerebral blood flow in human striate cortex, demonstrated by positron emission tomography. *J. Neurophysiol.* **51,** 1109–1120 (1984).
38. Kleinfeld, D., Mitra, P. P., Helmchen, F. & Denk, W. Fluctuations and stimulus-induced changes in blood flow observed in individual capillaries in layers 2 through 4 of rat neocortex. *Proc. Natl Acad. Sci. USA* **95,** 15741–15746 (1998).
39. Chaigneau, E. *et al.* The relationship between blood flow and neuronal activity in the rodent olfactory bulb. *J. Neurosci.* **27,** 6452–6460 (2007).
40. Cauli, B. *et al.* Cortical GABA interneurons in neurovascular coupling: relays for subcortical vasoactive pathways. *J. Neurosci.* **24,** 8940–8949 (2004).
41. Peppiatt, C. M., Howarth, C., Mobbs, P. & Attwell, D. Bidirectional control of CNS capillary diameter by pericytes. *Nature* **443,** 700–704 (2006).

Supplementary Information is linked to the online version of the paper at www.nature.com/nature.

Acknowledgements We thank T. Murphy, T. Phillips and Y. Tian Wang for reading an earlier version of the manuscript. T34 was a gift from V. L. Schuster and Y. Chi. This work was supported by an operating grant from the Canadian Institutes of Health Research. B.A.M. is a Canada Research Chair and a Michael Smith Foundation for Health Research (MSFHR) Distinguished Scholar. G.R.J.G. is supported by fellowships from the Alberta Heritage Foundation for Medical Research, MSFHR and the Natural Science and Engineering Council of Canada. H.B.C. is supported by postdoctoral fellowships from Wilms Foundation and the Heart and Stroke Foundation of Canada.

Author Contributions G.R.J.G. and B.A.M. designed the imaging experiments and wrote the manuscript. G.R.J.G. performed the imaging experiments and analysis, took slice p_{O2} measurements and tested the effects of synaptic activation on vasomotion. H.B.C., G.R.J.G. and B.A.M. designed the lactate and PGE_2 experiments. H.B.C. and B.A.M. designed the immunohistochemistry experiments. H.B.C. performed the lactate and PGE_2 measurements and analysis and the immunohistochemistry. R.L.R. performed the extracellular field recordings examining adenosine tone. G.C.R.E.-D. designed and synthesized the calcium cage. All authors helped to edit the manuscript.

Author Information Reprints and permissions information is available at www.nature.com/reprints. Correspondence and requests for materials should be addressed to B.A.M. (bmacvicar@brain.ubc.ca).

©2008 Macmillan Publishers Limited. All rights reserved

METHODS

Slice preparation and O_2 conditions. Sprague–Dawley rats were anaesthetized with halothane (Sigma), decapitated and the brains removed into ice-cold slicing solution containing (in mM): NaCl, 87; KCl, 2.5; $NaHCO_3$, 25; $CaCl_2$, 0.5; $MgCl_2$, 7; NaH_2PO_4, 1.25; glucose, 25; sucrose, 75; saturated with 95% O_2/5% CO_2. Transverse hemi-sections, 400 μm thick, were sliced (Leica vibratome) and incubated at 34 °C in ACSF containing (in mM): NaCl, 126; KCl, 2.5; $NaHCO_3$, 26; $CaCl_2$, 2.0; $MgCl_2$, 1.5; NaH_2PO_4, 1.25; glucose, 10; saturated with 95% O_2/5% CO_2 for 60 min. For experiments slices were at 22–24 °C and perfused at ~2 ml min^{-1}. 20% O_2 provided a p_{O2} on the low end of physiological[16] (Supplementary Fig. 2). Healthy slices can be maintained in 20% O_2 (ref. 42).

Imaging and uncaging. Images were acquired between 50 and 100 μm deep into the slice. Rhod-2 was excited at 835 nm (~3 mW after the objective) and fluorescence was detected with a PMT after passing through a 605-nm (55-nm band-pass) emission filter. For uncaging, the laser was tuned to 730 nm, which also excites rhod-2 (ref. 43). The laser power was carefully increased (~40 mW after the objective) until a Ca^{2+} signal, characteristic of internal release, occurred within astrocytes, triggering a Ca^{2+} wave. The nonlinearity of two-photon microscopy[44] ensures no uncaging occurs during rhod-2 excitation.

For NADH excitation the laser was tuned to 740 nm[14] (~30 mW after the objective) and fluorescence was detected with a PMT after passing through a 450-nm (30-nm band-pass) emission filter. Time series NADH images were acquired every 30 s. NADH *z*-stacks (one control and then one treatment) were acquired continuously. Although exhibiting identical spectral properties to NADH, NADPH is thought to contribute little to the fluorescence signal[45,46].

Lactate and PGE_2 measurements. Protocols in suppliers' instructions were followed for the PGE_2 ELISA and the lactate assays. In both, tetrodotoxin (TTX, 1 μM) and 3,7-dihydro-1-methyl-3-(2-methylpropyl)-1H-purine-2,6-dione (IBMX, 100 μM) were added to dampen neuronal activation and preserve cAMP, respectively. cAMP facilitates glycogen breakdown[47] which is important for astrocyte glycolysis[48]. We confirmed that the same effects occur, yet at higher values, without these compounds.

Immunohistochemistry. Twenty-micrometre sections were used for immunostaining as described[49]. Sections were incubated in blocking solution containing 0.5% BSA and 0.2% Triton X-100 in 0.1 M PBS for 30 min. Sections were incubated overnight at 4 °C with primary antibodies against GFAP (1:1,000; Sigma), MAP2 (1:1,000; Chemicon), COX1 (1:200; Santa Cruz Biotechnology), COX2 (1:200; Santa Cruz Biotechnology), or PGT (1:100; Alpha diagnostic). Sections were then incubated with secondary antibodies: FITC-conjugated mouse anti-rabbit IgG, FITC-conjugated donkey anti-mouse IgG, rhodamine-conjugated rabbit anti-goat IgG or rhodamine-conjugated goat anti-mouse IgG at room temperature for 2 h in darkness (all secondary antibodies from Santa Cruz Biotechnology).

Electrophysiology. For extracellular recordings examining adenosine, slices were maintained at 34 °C and bubbled with an O_2 treatment 45 min before experimentation. Field excitatory postsynaptic potentials (fEPSPs) were evoked by stimulating the hippocampal CA3–CA1 pathway using a concentric bipolar electrode (Frederick Haer Co.) and were acquired in stratum radiatum. fEPSPs were evoked every 30 s and were analysed for slope (mV ms^{-1}) (see ref. 33 for details). Responses were normalized to the control mean. A second response, 50 ms after the first, was evoked for the paired-pulse. The paired-pulse ratio equals the average of ten sweeps during DPCPX/average of ten sweeps immediately before DPCPX.

To test synaptic activation in vasomotion, a stimulating electrode and recording electrode were positioned ~250 μm apart in the CA3–CA1 pathway, straddling the vessel. A 10–20-Hz stimulation train 350–1,000 ms in duration was repeated 5–10 times at a rate of 0.5–1 Hz. Once a constriction was observed in high O_2, the same stimulation protocol was used in low O_2 to evoke dilation. Forty minutes equilibration was allowed when the p_{O2} was changed.

Data collection, analysis and statistics. An image (512 × 512 pixels) was collected in 393.2–983.4 ms, using 8-line averaging. Lumen diameter measurements were made at multiple sites along the vessel. Fluorescence signals were defined as $F/F_0\,(\%) = [(F_1 - B_1)/(F_0 - B_0)]100$, where F_1 and F_0 are fluorescence at a given time and the control period mean, respectively. B_1 and B_0 are the corresponding background fluorescence signals. Background values were taken from the neuropil for rhod-2 and the vessel lumen for NADH. Pseudo-colour images show absolute changes in fluorescence (ImageJ, 16-colour linear Lut). Experimental values are the mean ± s.e.m.; baseline equals 100%; *n* is the number of experiments conducted. Lumen diameter changes: 90% means a reduction in diameter by 10% and 110% means an increase in diameter by 10%. Statistical tests were either a two-tailed Student's *t*-test or an ANOVA with a Neumann–Keuls post-hoc test for comparison between multiple groups. $P < 0.05$ was accepted as statistically significant (asterisk, $P < 0.05$; double asterisk, $P < 0.01$).

Drugs. Sigma supplied tACPD, applied for 5–10 min; lactate, applied for 5–10 min and pH-corrected to 7.4; sodium-oxamate and sodium-iodoacetate, applied continuously with 15 min incubation (iodoacetate exposure of ~30 min generated an 'anoxic-depolarization-like' wave causing vessel spasms; tACPD was assessed before this event); indomethacin, applied continuously with 20 min incubation; IBMX, present during the release assays; U46619, applied continuously with 20 min incubation. Tocris supplied DPCPX, applied continuously; CGS21680, applied continuously with 20 min incubation. Alamone labs supplied tetrodotoxin, present during release assays. Cayman Chemicals supplied PGE_2, applied for 5 min. Invitrogen supplied rhod-2/AM. DMNPE-4/AM was synthesized by G. Ellis-Davies. T34, puffed from a pipette or bath applied, was a gift from V. L. Schuster.

42. D'Agostino, D. P., Putnam, R. W. & Dean, J. B. Superoxide ($\bullet O_2^-$) production in CA1 neurons of rat hippocampal slices exposed to graded levels of oxygen. *J. Neurophysiol.* **98,** 1030–1041 (2007).
43. Xu, C., Zipfel, W., Shear, J. B., Williams, R. M. & Webb, W. W. Multiphoton fluorescence excitation: new spectral windows for biological nonlinear microscopy. *Proc. Natl Acad. Sci. USA* **93,** 10763–10768 (1996).
44. Denk, W. Two-photon scanning photochemical microscopy: mapping ligand-gated ion channel distributions. *Proc. Natl Acad. Sci. USA* **91,** 6629–6633 (1994).
45. Klaidman, L. K., Leung, A. C. & Adams, J. D. Jr. High-performance liquid chromatography analysis of oxidized and reduced pyridine dinucleotides in specific brain regions. *Anal. Biochem.* **228,** 312–317 (1995).
46. Vishwasrao, H. D., Heikal, A. A., Kasischke, K. A. & Webb, W. W. Conformational dependence of intracellular NADH on metabolic state revealed by associated fluorescence anisotropy. *J. Biol. Chem.* **280,** 25119–25126 (2005).
47. Sorg, O. & Magistretti, P. J. Characterization of the glycogenolysis elicited by vasoactive intestinal peptide, noradrenaline and adenosine in primary cultures of mouse cerebral cortical astrocytes. *Brain Res.* **563,** 227–233 (1991).
48. Brown, A. M. & Ransom, B. R. Astrocyte glycogen and brain energy metabolism. *Glia* **55,** 1263–1271 (2007).
49. Ryu, J. K. *et al.* Microglial activation and cell death induced by the mitochondrial toxin 3-nitropropionic acid: *in vitro* and *in vivo* studies. *Neurobiol. Dis.* **12,** 121–132 (2003).

©2008 Macmillan Publishers Limited. All rights reserved